AGU PUBLICATIONS

Geophysical Research Letters

RESEARCH LETTER
10.1002/2015GL065720

Special Section:
First Results from the MAVEN Mission to Mars

Estimation of the spatial structure of a detached magnetic flux rope at Mars based on simultaneous MAVEN plasma and magnetic field observations

Takuya Hara[1], David L. Mitchell[1], James P. McFadden[1], Kanako Seki[2], David A. Brain[3], Jasper S. Halekas[4], Yuki Harada[1], Jared R. Espley[5], Gina A. DiBraccio[5], John E. P. Connerney[5], Lailla Andersson[3], Christian Mazelle[6,7], and Bruce M. Jakosky[3]

[1]Space Sciences Laboratory, University of California, Berkeley, California, USA, [2]Solar-Terrestrial Environment Laboratory, Nagoya University, Nagoya, Japan, [3]Laboratory for Atmospheric and Space Physics, University of Colorado Boulder, Boulder, Colorado, USA, [4]Department of Physics and Astronomy, University of Iowa, Iowa City, Iowa, USA, [5]NASA Goddard Space Flight Center, Greenbelt, Maryland, USA, [6]CNRS, Institut de Recherche en Astrophysique et Planétologie, Toulouse, France, [7]Université Paul Sabatier, Toulouse, France

Key Points:
- First detection by MAVEN of a detached flux rope at Mars
- Detached flux rope includes planetary origin heavy ion populations
- Observed location is downstream from the strong crustal magnetic fields

Correspondence to:
T. Hara,
hara@ssl.berkeley.edu

Citation:
Hara, T., et al. (2015), Estimation of the spatial structure of a detached magnetic flux rope at Mars based on simultaneous MAVEN plasma and magnetic field observations, *Geophys. Res. Lett.*, *42*, doi:10.1002/2015GL065720.

Received 12 AUG 2015
Accepted 1 SEP 2015

Abstract Simultaneous Mars Atmosphere and Volatile EvolutioN mission (MAVEN) plasma and magnetic field observations reveal a detached magnetic flux rope in the Martian induced magnetosphere. The flux rope was identified by an increase in the magnetic field amplitude accompanied by smooth vector rotations. In addition, MAVEN observed a pronounced ion composition change across the structure, with solar wind ions dominating outside and planetary ions dominating within. Grad-Shafranov reconstruction is applied to determine the two-dimensional spatial structure of the flux rope. The event occurred near the dusk terminator, downstream from strong crustal magnetic fields. One possibility is that the flux rope was created by magnetic reconnection associated with interplanetary and/or crustal magnetic fields. A weak interplanetary coronal mass ejection (ICME) arrived at Mars a few hours before the event. A pressure pulse and turbulent magnetic fields due to the ICME might be responsible for driving magnetic reconnection to detach the flux rope from the crustal source.

1. Introduction

Magnetic flux ropes are helical magnetic field structures observed throughout the solar system [e.g., *Russell and Elphic*, 1979]. Flux ropes were first observed around Mars by the Mars Global Surveyor (MGS) spacecraft [e.g., *Cloutier et al.*, 1999; *Vignes et al.*, 2004; *Briggs et al.*, 2011], even though Mars lacks a global intrinsic magnetic field [e.g., *Acuña et al.*, 1998]. The plasma environments around unmagnetized planets, such as Mars and Venus, are generally controlled by solar wind conditions, including the interplanetary magnetic field (IMF) strength and orientation. However, the IMF and associated draped magnetic fields may not be the only source of magnetic flux ropes at Mars, because Mars possesses strong localized crustal magnetic fields [e.g., *Acuña et al.*, 1998, 1999]. The crustal magnetic sources are distributed nonuniformly, and their strengths and orientations with respect to the IMF vary continuously as the planet rotates. The strongest crustal magnetic fields are located in the southern hemisphere around 180° longitude [e.g., *Acuña et al.*, 1999; *Connerney et al.*, 2005]. Based on magnetic field measurements by MGS, Martian crustal magnetic field models have been developed by several authors [e.g., *Cain et al.*, 2003; *Morschhauser et al.*, 2014]. Large-scale, isolated flux ropes have previously been observed downstream from strong crustal magnetic fields [e.g., *Brain et al.*, 2010; *Morgan et al.*, 2011; *Hara et al.*, 2014a]. *Beharrell and Wild* [2012] reported that magnetic field enhancements, mostly associated with flux rope signatures, were concentrated at solar zenith angles between 90° and 100° in the southern hemisphere. Moreover, such events were repeatedly detected when strong crustal magnetic fields were located on the dayside, upstream of the southern polar region [*Beharrell and Wild*, 2012].

If flux ropes detach, they can carry ionospheric plasma away from the planet. Over time, this and other escape phenomena resulting from the direct interaction of the solar wind with the Martian upper atmosphere might have contributed significantly to Martian atmospheric evolution and climate change [e.g., *Jakosky and Phillips*, 2001]. Phobos-2 and Mars Express (MEX) measurements have directly shown planetary ions escaping into interplanetary space [e.g., *Lundin et al.*, 1989; *Barabash et al.*, 2007]. Based on the MGS observations, *Brain*

et al. [2010] proposed that detached flux ropes might account for as much as 10% of the total present-day ion escape from Mars. More recently, *Hara et al.* [2014a, 2014b] estimated lower limits to the ion escape rate due to large-scale magnetic flux ropes using Grad-Shafranov reconstruction (GSR), which can constrain the rope's two-dimensional magnetohydrostatic structure based on measurements from a single spacecraft [e.g., *Hu and Sonnerup*, 2001, 2002; *Hasegawa et al.*, 2006]. These lower limits, also based on MGS data, are on the order of 10^{22}–10^{23} s^{-1}. The current global ion escape rate from all mechanisms is uncertain by at least an order of magnitude, but these results indicate that detached flux ropes can contribute 1–10% of the total escape [*Hara et al.*, 2014a, 2014b]. Because of the lack of ion measurements by MGS, previous studies had to assume an ionospheric plasma density within the observed flux ropes. Hence, the simultaneous ion and magnetic field measurements by the Mars Atmosphere and Volatile EvolutioN mission (MAVEN) present an opportunity to derive a more reliable estimate of ion escape associated with flux ropes.

In this paper, we first present simultaneous MAVEN plasma and magnetic field observations that reveal a magnetic flux rope detached from the Martian ionosphere. We then apply the GSR technique to estimate the rope's two-dimensional spatial structure and axial orientation. Because this is the first opportunity to apply the GSR technique with simultaneous measurements of multiple ion species, we investigate three different cases and compare the results. We use these results to explore possible formation mechanisms for the observed flux rope and to estimate the associated ion escape rate.

2. MAVEN Instrumentation

MAVEN is the first NASA orbiter mission dedicated to investigate the upper atmosphere and plasma environment around Mars [*Jakosky et al.*, 2015]. MAVEN was launched on 18 November 2013 and entered into orbit around Mars on 22 September 2014. MAVEN has a 75° inclination science mapping orbit with a periapsis (apoapsis) altitude of ~150 km (~6200 km). The orbital period is approximately 4.5 h. The MAVEN science payload makes simultaneous measurements of ions, electrons, and neutrals and magnetic field. In this study, we use data obtained from the Suprathermal and Thermal Ion Composition (STATIC) analyzer [*McFadden et al.*, 2015], the Solar Wind Ion Analyzer (SWIA) [*Halekas et al.*, 2013], the Solar Wind Electron Analyzer (SWEA) [*Mitchell et al.*, 2015], and the Magnetometer (MAG) [*Connerney et al.*, 2015]. MAG data are utilized to identify a magnetic flux rope. STATIC and SWEA are utilized to investigate the behavior of planetary ions and electrons across the flux rope. Since STATIC can measure the ion mass composition as well as the energy and angular distributions as often as every 4–16 s [*McFadden et al.*, 2015], we are able to estimate the composition, density, bulk velocity, and temperature of planetary ions within the flux rope for the first time. SWIA is utilized to infer the solar wind plasma properties during the event.

3. MAVEN Observations of Detached Flux Rope Event on 26 December 2014

Figure 1 shows an overview of the detached magnetic flux rope event on 26 December 2014. The spacecraft crossed the bow shock at an altitude of 4800 km (13:22 UT), as it was traveling inbound toward periapsis (Figure 2a). As the spacecraft descended from ~3000 to ~2700 km altitude, the flux of the solar wind plasma gradually decreased in both intensity and energy (Figures 1a and 1d). MAVEN crossed the magnetic pileup boundary (MPB) at around 13:54:20, as evidenced by the appearance of planetary O_2^+ (Figure 1b) and the decrease in magnetic field fluctuations (Figure 1g). Between 13:57:50 and 13:58:10, shown by the magenta bar between Figures 1e and 1f, the observed magnetic field amplitude (solid black line) was enhanced and its direction rotated smoothly as shown in Figures 1f and 1g. Minimum variance analysis (MVA) [e.g., *Sonnerup and Scheible*, 1998] of the magnetic field data during the event yields the hodograms shown in Figure 3. The hodogram clearly shows that magnetic field vector rotates smoothly in the plane perpendicular to the minimum variance axis (B_k) in Figure 3a. The eigenvalue ratio between the intermediate and minimum variance axis is approximately 41.1 (i.e., $\lambda_j/\lambda_k = 41.1$), which allows us to confidently identify this feature as a magnetic flux rope [e.g., *Russell and Elphic*, 1979; *Vignes et al.*, 2004]. A similar but less pronounced magnetic field signature is observed around 14:04 UT.

Simultaneous ion and electron measurements by STATIC, SWIA, and SWEA reveal the plasma signature associated with the flux rope. The ion mass composition and energy distribution are distinctly different inside and outside the flux rope (Figures 1a and 1c). Low-mass ions (protons and alphas) are attenuated within the flux rope and have an average energy 10 times lower than outside. At the same time, high-mass ions (primarily O^+ and O_2^+), which are of planetary origin, are enhanced (Figures 1b and 1c). During the event, the plasma

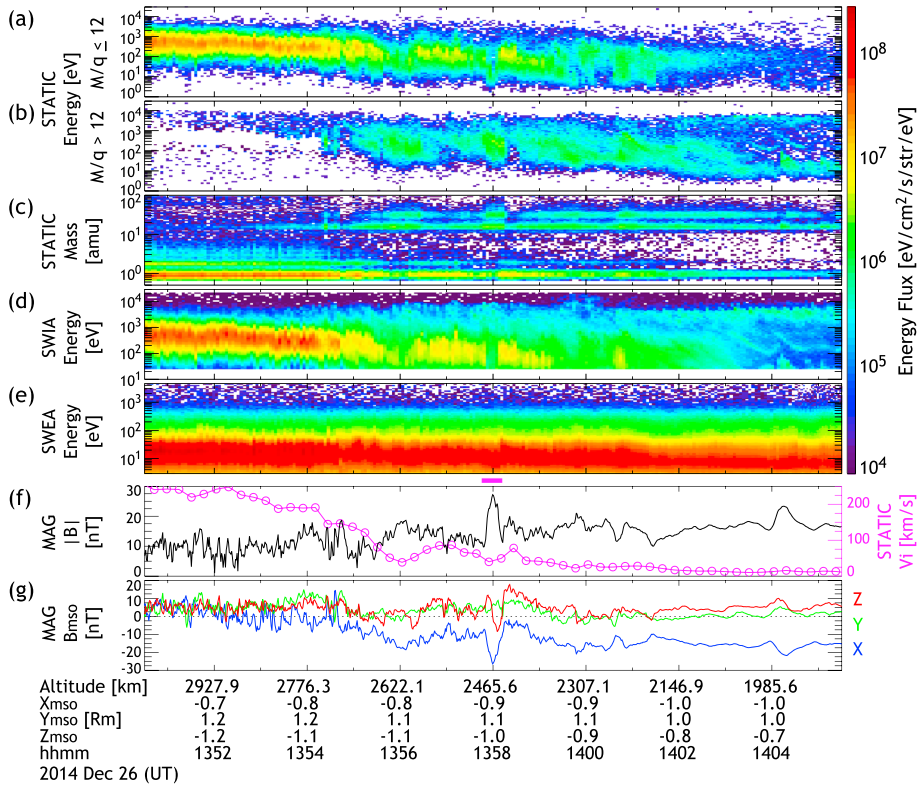

Figure 1. Overview of time series plot of detached magnetic flux rope event observed by MAVEN on 26 December 2014. STATIC (a) light ($M/q \leq 12$) and (b) heavy ($M/q > 12$) ions omnidirectional energy, (c) mass, (d) SWIA ion, and (e) SWEA electron omnidirectional energy spectra as a function of time, where M means the ion mass and q is the electric charge. Magnetic field (f) amplitude (black line in the left vertical axis) and (g) vector components in the Mars-centered Solar Orbital (MSO) coordinate system measured by MAG. The MSO coordinate system is defined with the X_{mso} axis toward the Sun, the Z_{mso} axis perpendicular to the ecliptic pointing to the northern hemisphere, and the Y_{mso} axis completing the right-hand system. The magenta bar between Figures 1e and 1f is an event time period when the detached magnetic flux rope is observed. The density-weighted ion bulk flow speed (V_i, magenta), obtained from the STATIC D1 data (16 s cadences), is overlaid in Figure 1f in the right vertical axis. It is used in the GSR technique (see section 4).

β (the ratio of the plasma pressure relative to the magnetic pressure) is smaller than 1. All ion species are included to compute the plasma pressure in this study. Note that within the flux rope, heavy ion energies are between ~50 and ~1000 eV, while proton energies are ~10 eV. This is consistent with an approximately common bulk flow speed of several tens of km/s, which is slower than the bulk flow speed of ~110 km/s outside of the rope. (The spacecraft velocity was 2.8 km/s during these measurements.) STATIC measurements also exhibit energy-dispersed planetary heavy ion signatures [see *Halekas et al.*, 2015] mostly during the transition region between 13:55 and 14:05. SWIA omnidirectional energy spectra, which do not discriminate mass, show a reduced ion flux from 25 to ~1000 eV (Figure 1d). These results suggest that the flux rope was formed in the Martian ionosphere. Although ion measurements show significant changes across the flux rope, there is no obvious signature in 3–4600 eV electrons (Figure 1e). There is a slight shift in the electron energy distribution just after MAVEN exited the flux rope, but similar signatures are observed at other locations that are not associated with flux ropes.

This event was observed on the duskside of the induced magnetosphere, downstream from the terminator plane (Figures 2b and 2c). The flux rope was observed at an altitude of ~2500 km, which is more than 5 times higher than previous flux rope observations by MGS [e.g., *Vignes et al.*, 2004; *Briggs et al.*, 2011]. The crustal magnetic field amplitude at this location is expected to be small (~1 nT) [*Morschhauser et al.*, 2014] compared with the measured magnetic field amplitude (~10 nT). However, interestingly, strong crustal magnetic fields in the southern hemisphere near 180° longitude were located around the dusk terminator (Figure 2b). Taking into account the solar wind flow direction, the observed location of the flux rope is approximately downstream

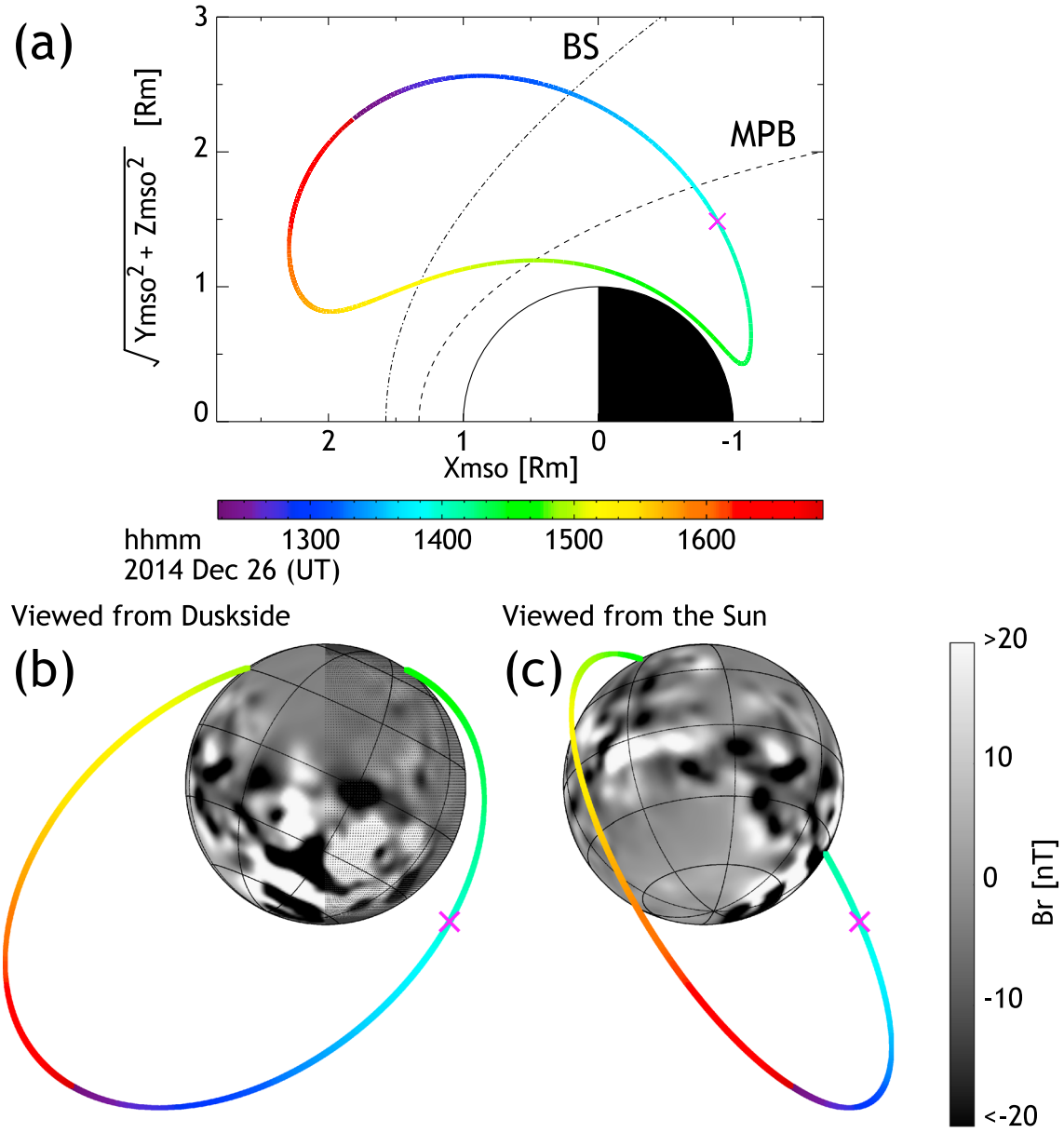

Figure 2. (a) The MAVEN orbital projection onto cylindrical X_{mso}, $\sqrt{Y_{mso}^2 + Z_{mso}^2}$ coordinates on 26 December 2014. MAVEN moves clockwise, and the rainbow colors of spacecraft trajectory correspond to the time of its location, as shown in the rainbow color bar. The dash-dotted and dashed lines describe the average positions of the bow shock (BS) and the magnetic pileup boundary (MPB) [*Edberg et al.*, 2008]. The MAVEN orbit tracks viewed from (b) duskside and (c) the Sun are also shown onto the crustal magnetic field map. Gray scale background indicates a radial component of crustal field model developed by *Morschhauser et al.* [2014] at 400 km altitude, as shown by gray scale color bar in the bottom right corner. A globe is gridded every 45° (30°) longitude (latitude). A right-half globe shaded on Figure 2b means that the spacecraft is in the eclipse; i.e., a left-half globe is illuminated by the Sun. The detached magnetic flux rope event is detected at the magenta cross.

from these strong crustal magnetic fields. Because the flux rope is estimated to be moving much faster than the local escape velocity (< 4 km/s), it is likely that the rope is detached from the crustal sources at least and escaping into interplanetary space.

4. Estimation of Spatial Structure Based on the Grad-Shafranov Reconstruction Technique

In this section, we attempt to estimate the spatial structure and axial orientation of the observed magnetic flux rope using Grad-Shafranov reconstruction (GSR). This technique makes it possible to recover the magne-

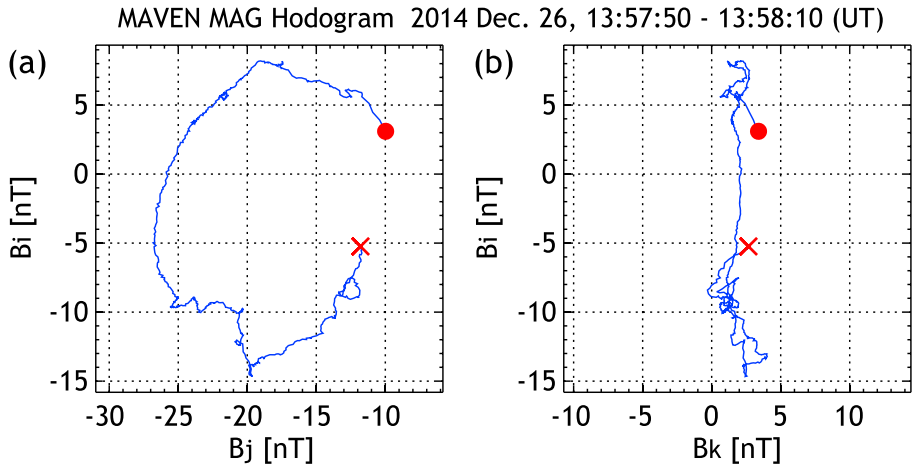

Figure 3. Hodograms of the detached magnetic flux rope event observed by MAVEN between 13:57:50 and 13:58:10 UT on 26 December 2014 in the minimum variance analysis (MVA) coordinate system, where B_i, B_j, and B_k components refer to the maximum, intermediate, and minimum variance axes, respectively. Red circles (crosses) are start (end) points, respectively.

tohydrostatic spatial structure from a single-spacecraft time series of plasma and magnetic field data, under the assumption that the structure is two dimensional and time independent [e.g., *Sturrock*, 1994; *Sonnerup and Guo*, 1996]. The GSR technique has been used for decades to recover various magnetohydrostatic structures, including flux ropes observed in interplanetary space (often known as magnetic clouds) [e.g., *Hau and Sonnerup*, 1999; *Hu and Sonnerup*, 2002] and in Earth's magnetosphere (often called flux transfer events) [e.g., *Sonnerup et al.*, 2004; *Hasegawa et al.*, 2006].

Assuming the structure to be two dimensional, there is an invariant axis z (the flux rope axis), along which the spatial gradient is much smaller than in the orthogonal directions, x and y. If we can find such a frame, the force balance equation between the magnetic tension and the total pressure gradient in the MHD framework, $\boldsymbol{j} \times \boldsymbol{B} = \nabla p$, can be reduced to the GS equation [e.g., *Sturrock*, 1994; *Hau and Sonnerup*, 1999; *Sonnerup et al.*, 2006]:

$$\nabla^2 A = \frac{\partial^2 A}{\partial x^2} + \frac{\partial^2 A}{\partial y^2} = -\mu_0 \frac{\mathrm{d}P_t(A)}{\mathrm{d}A}, \tag{1}$$

where A is the z component of the vector potential and P_t is the transverse pressure, which is the sum of the plasma pressure and axial magnetic pressure: $P_t = p + B_z^2/(2\mu_0)$. Since p and B_z are functions of A alone, P_t is also uniquely determined as a function of A. The vector magnetic field $\boldsymbol{B}$ can be calculated from the vector potential A: $\boldsymbol{B} = [\partial A/\partial y, -\partial A/\partial x, B_z(A)]$. In order to recover the spatial structure, the GS equation (1) is solved numerically as a Cauchy (i.e., spatial initial value) problem by using the plasma and magnetic field data along the spacecraft path (i.e., $y = 0$ in the GSR x-y plane) [e.g., *Hau and Sonnerup*, 1999]. This is usually performed in the de Hoffmann-Teller (HT) frame, because the HT velocity, $\boldsymbol{V}_{\mathrm{HT}}$, allows the time series data to be converted into spatial information along the spacecraft path. Hence, the value of A along the GSR x axis can be computed from the observed GSR y component of the magnetic field, B_y, via the spatial integration:

$$A(x,0) = \int_0^x \frac{\partial A}{\partial \xi}\mathrm{d}\xi = -\int_0^x B_y(\xi,0)\mathrm{d}\xi. \tag{2}$$

Spatial integration, $\mathrm{d}\xi$, can be transformed into time integration via the following relation: $\mathrm{d}\xi = -\boldsymbol{V}_{\mathrm{HT}} \cdot \hat{\boldsymbol{x}}\mathrm{d}t$, where $\hat{\boldsymbol{x}}$ is a unit vector along the projection of $-\boldsymbol{V}_{\mathrm{HT}}$ onto the plane perpendicular to the invariant axis. The detailed methodology of the GSR technique is fully described in previous studies [e.g., *Hau and Sonnerup*, 1999; *Hu and Sonnerup*, 2002; *Hasegawa et al.*, 2012], and we adopt the same procedure in this study.

After recovering the axial z magnetic field map using the GSR technique, we tested three different cases to investigate influence of the plasma pressure included inside the flux rope. Case 1 assumes the force-free approximation; that is, the contribution of the plasma pressure is ignored ($p = 0$). The remaining two cases

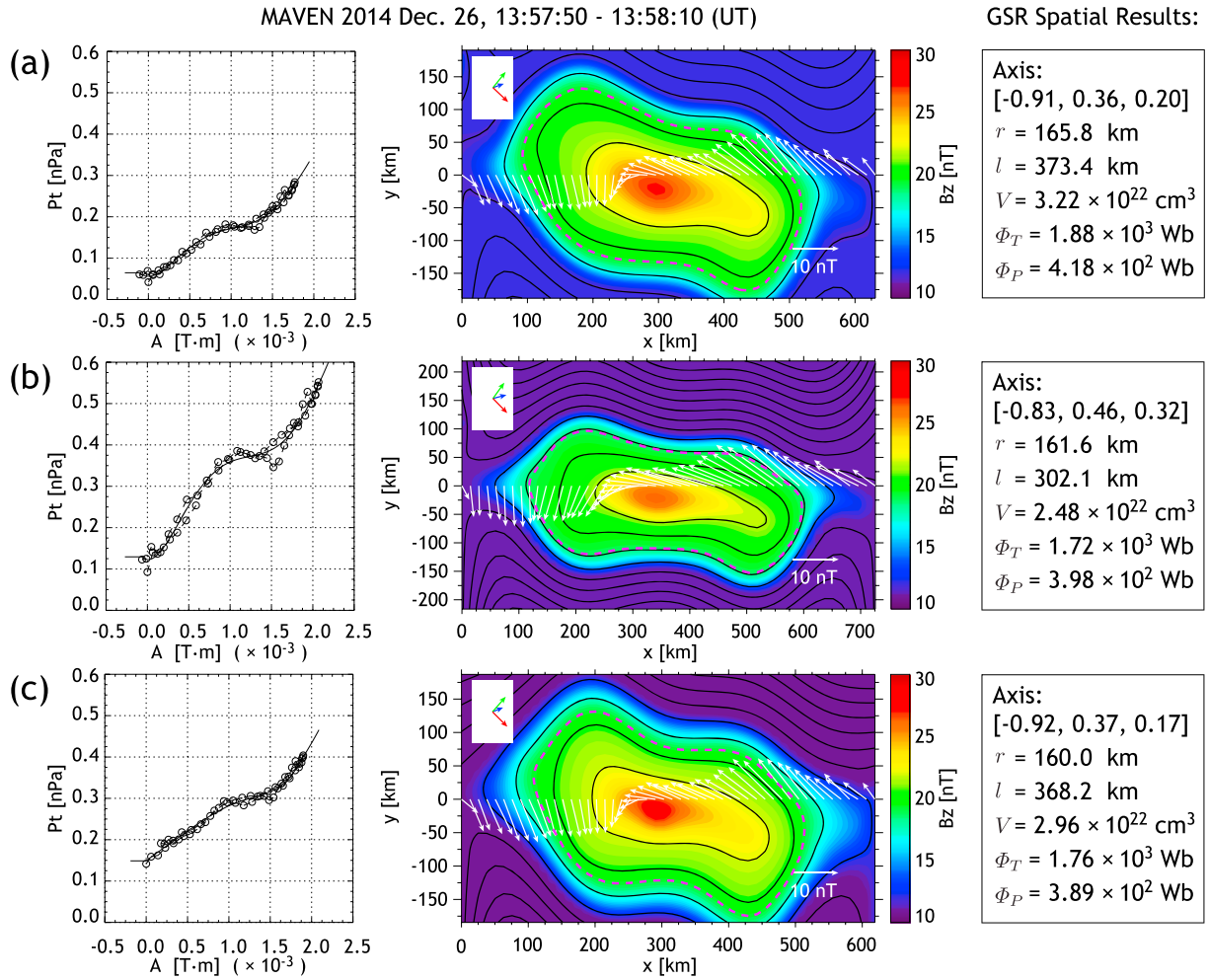

Figure 4. Results from the GSR technique based on the MAVEN plasma and magnetic field measurements for (a) Case 1, (b) Case 2, and (c) Case 3, respectively. The transverse pressure P_t plotted as a function of the magnetic vector potential A (left column). Open circles are the MAVEN observations, and the solid curves denote the fitted polynomials. The reconstructed two-dimensional maps of transverse magnetic field lines (black curves) with an axial magnetic field B_z in color (right column). MAVEN was traveling (time progressed) from left to right along the line $y = 0$. Overlaid white arrows represent the transverse magnetic field components measured by MAVEN. The blue, green, and red arrows shown at top left corner on the reconstructed map are the projections of X_{mso}, Y_{mso}, and Z_{mso} axes, respectively. The dashed magenta curve is the flux rope boundary used in this study. The definition of the flux rope boundary is given in the text. The spatial properties of the flux rope derived from the GSR technique are shown on the right of each case.

are nonforce-free conditions ($p > 0$). In Case 2, the plasma pressure is assumed to balance the observed magnetic pressure ($p = nk_BT = B^2/(2\mu_0)$, where μ_0 is the magnetic permeability of free space). In Case 3, the total plasma pressure summed over all ion species is used based on STATIC observations ($p = nk_BT$, where n is a plasma number density, k_B is a Boltzmann constant, and T is a plasma temperature). The pressure computed in Case 3 tends to be smaller than the pressure assumed in Case 2. Based on the SWEA measurements, the ratio of the electron pressure to the total plasma pressure is computed to be < 13% during the event. Hence, the electron pressure contribution can be safely ignored when determining spatial structure by the GSR technique for this event. Furthermore, we note that the ion density-weighted average HT velocity $\boldsymbol{V}_{HT}$ is used in all cases, since STATIC measured multiple ion species within the flux rope. This is computed to be $\boldsymbol{V}_{HT} = [-40.2, -7.6, -16.4]$ km/s in the MSO coordinates for this event.

Figure 4 shows the axial (z) magnetic field component in the plane orthogonal to the flux rope axis, estimated by the GSR technique for each case. Comparing Cases 1 and 2, we can see the influence of plasma pressure, which results in a smaller, more elongated x-y cross section. The spatial structure for Case 3, which is based on STATIC measurements, more closely resembles that of Case 1, indicating that the contribution of plasma pressure is not significant in characterizing the reconstructed shape, at least in this event. The spatial properties obtained from the GSR technique for each case are summarized on the right of the reconstructed map

in Figure 4. The flux rope *z* axis (Figure 4) is nearly aligned with the Sun-Mars line (MSO *x* axis) for all cases. The differences of the estimated flux rope *z* axis among three cases are approximately between 2° and 11°. The dashed magenta line onto Figure 4 is the flux rope boundary defined as a surface where the reconstructed axial field strength is 50% of the core field value in this study. The equivalent radius (*r*) is the radius of a circle with the same area as the reconstructed cross section (within the dashed magenta line). The rope length (*l*) along the flux rope *z* axis is estimated from the MAVEN flight distance in the HT frame, assuming that the reconstructed spatial structure is maintained at least over the time interval when MAVEN was inside the flux rope. These flux rope volumes (*V*) are comparable to previous volume estimates for magnetic flux ropes detected by MGS near the Martian ionosphere around 400 km altitude [*Hara et al.*, 2014a, 2014b]; however, the core axial field strength of this event is significantly weaker than that of MGS ionospheric events [e.g., *Brain et al.*, 2010; *Briggs et al.*, 2011; *Hara et al.*, 2014b]. We also computed the toroidal (Φ_T) and poloidal (Φ_P) magnetic fluxes contained inside the flux rope based on previous studies [e.g., *Qiu et al.*, 2007; *Hu et al.*, 2014]. These results are noted in Figure 4.

5. Summary and Discussions

In this paper, we report on MAVEN plasma and magnetic field observations of a magnetic flux rope around Mars. This event was observed in the southern hemisphere of the Martian induced magnetosphere, downstream of the terminator plane and a region of strong crustal magnetic fields (Figure 2). As MAVEN traversed the flux rope, STATIC measured an enhancement of planetary ions and a concurrent suppression of solar wind ions. We infer that the observed flux rope was formed in a region with access to planetary ions but not to magnetosheath ions. One likely such location is on closed magnetic field lines within the Martian ionosphere. We applied the GSR technique using MAVEN plasma and magnetic field data to estimate the two-dimensional spatial structure of the flux rope. We found that the rope's axis is nearly aligned with the Sun-Mars line and that plasma pressure does not significantly influence the rope's spatial structure for this event (Figure 4).

A region of strong crustal magnetic fields was located near the dusk terminator and upstream of the spacecraft when MAVEN observed the flux rope, as shown in Figure 2b. Previous studies report that MGS detected a large number of magnetic flux ropes around the Martian ionosphere at about 400 km altitude [e.g., *Briggs et al.*, 2011; *Beharrell and Wild*, 2012; *Hara et al.*, 2014b]. This altitude is low enough that it is difficult to confidently determine whether or not the observed flux ropes are detached from crustal magnetic fields. However, the event in this study was observed above 2400 km altitude. Furthermore, STATIC observations indicate that the ion populations inside the flux rope are moving approximately antisunward with a bulk velocity that is much larger than the escape velocity. These observations are consistent with a scenario in which the flux rope detached from crustal magnetic fields at the surface, possibly via magnetic reconnection [e.g., *Halekas et al.*, 2009; *Brain et al.*, 2010; *Hara et al.*, 2014b; *Harada et al.*, 2015].

Here we estimate ion escape rates associated with the observed flux rope, based on the GSR results and STATIC ion observations. The measured ion densities within the flux rope are 4.6 cm^{-3} for H^+, 4.2 cm^{-3} for O^+, and 4.4 cm^{-3} for O_2^+. To estimate volume, we use the spatial properties obtained from the GSR technique for Case 3 described in the previous section. The plasma contents within the flux rope are computed to be 1.36×10^{23} ions for H^+, 1.23×10^{23} ions for O^+, and 1.30×10^{23} ions for O_2^+. Since MAVEN traverses the flux rope in 11.8 s, we can set lower limits to the ion escape rates, assuming that plasma within the flux rope is completely removed within this traversal time. These escape rates are 1.16×10^{22} s^{-1} for H^+, 1.04×10^{22} s^{-1} for O^+, and 1.11×10^{22} s^{-1} for O_2^+. MEX observations reveal that global ion escape rates are presently on the order of 10^{24} s^{-1} [e.g., *Barabash et al.*, 2007; *Nilsson et al.*, 2010; *Lundin et al.*, 2008, 2013]. Thus, a single detached magnetic flux rope instantaneously contributes >1% of the total ion escape rate from Mars. These estimates are comparable to those in previous GSR studies [e.g., *Hara et al.*, 2014a, 2014b].

We note that similar but broader and less pronounced ion signatures are observed by STATIC before the flux rope crossing that has been the focus of this study (Figure 1b). Judging from the energy width of planetary heavy ion populations (Figure 1b), these ions are hot and have gyroradii (~150 km for O^+) that are comparable to the estimated spatial scale of the flux rope (Figure 4), even though they are traveling along with the flux rope. Therefore, some planetary heavy ions measured across the structure might not be trapped inside the flux rope.

Finally, a weak interplanetary shock signature, possibly associated with an interplanetary coronal mass ejection (ICME), was detected by SWIA and MAG measurements around 12:00 UT on 26 December 2014, just a

few hours before the flux rope observations. Although the solar wind velocity jump was not large (~340 km/s to ~380 km/s), the solar wind density (~16 cm^{-3}), dynamic pressure (~4 nPa), and magnetic field amplitude (~8 nT) after the ICME shock arrival are approximately 2 times larger than before. Hence, the flux rope event in this study was observed when the ICME shock sheath in front of the interplanetary magnetic cloud passed through Mars. One possibility is that a pressure pulse combined with turbulent magnetic fields in the ICME shock sheath might be responsible for detaching a flux rope from the crustal source via magnetic reconnection. MAVEN observations of other flux rope events will be used to further our understanding of the physical mechanisms responsible for forming and detaching flux ropes at Mars.

Acknowledgments
The data used in this paper are publicly available in NASA's Planetary Data System. This work was carried out by the joint research programs of the Solar-Terrestrial Environment Laboratory, Nagoya University.

The Editor thanks two anonymous reviewers for their assistance in evaluating this paper. This work was supported by CNES for the part based on observations with MAVEN SWEA.

References

Acuña, M. H., et al. (1998), Magnetic field and plasma observations at Mars: Initial results of the Mars Global Surveyor mission, *Science*, *279*, 1676–1680, doi:10.1126/science.279.5357.1676.

Acuña, M. H., et al. (1999), Global distribution of crustal magnetization discovered by the Mars Global Surveyor MAG/ER experiment, *Science*, *284*, 790–793, doi:10.1126/science.284.5415.790.

Barabash, S., A. Fedorov, R. Lundin, and J.-A. Sauvaud (2007), Martian atmospheric erosion rates, *Science*, *315*, 501–503, doi:10.1126/science.1134358.

Beharrell, M. J., and J. A. Wild (2012), Stationary flux ropes at the southern terminator of Mars, *J. Geophys. Res.*, *117*, A12212, doi:10.1029/2012JA017738.

Brain, D. A., A. H. Baker, J. Briggs, J. P. Eastwood, J. S. Halekas, and T.-D. Phan (2010), Episodic detachment of Martian crustal magnetic fields leading to bulk atmospheric plasma escape, *Geophys. Res. Lett.*, *37*, L14108, doi:10.1029/2010GL043916.

Briggs, J. A., D. A. Brain, M. L. Cartwright, J. P. Eastwood, and J. S. Halekas (2011), A statistical study of flux ropes in the Martian magnetosphere, *Planet. Space Sci.*, *59*, 1498–1505, doi:10.1016/j.pss.2011.06.010.

Cain, J. C., B. B. Ferguson, and D. Mozzoni (2003), An $n = 90$ internal potential function of the Martian crustal magnetic field, *J. Geophys. Res.*, *108*(E2), 5008, doi:10.1029/2000JE001487.

Cloutier, P. A., et al. (1999), Venus-like interaction of the solar wind with Mars, *Geophys. Res. Lett.*, *26*(17), 2685–2688, doi:10.1029/1999GL900591.

Connerney, J. E. P., M. H. Acuña, N. F. Ness, G. Kletetschka, D. L. Mitchell, R. P. Lin, and H. Rème (2005), Tectonic implications of Mars crustal magnetism, *Proc. Natl. Acad. Sci. U.S.A.*, *102*, 14,970–14,975, doi:10.1073/pnas.0507469102.

Connerney, J. E. P., J. Espley, P. Lawton, S. Murphy, J. Odom, R. Oliversen, and D. Sheppard (2015), The MAVEN Magnetic Field Investigation, *Space Sci. Rev.*, doi:10.1007/s11214-015-0169-4.

Edberg, N. J. T., M. Lester, S. W. H. Cowley, and A. I. Eriksson (2008), Statistical analysis of the location of the Martian magnetic pileup boundary and bow shock and the influence of crustal magnetic fields, *J. Geophys. Res.*, *113*, A08206, doi:10.1029/2008JA013096.

Halekas, J. S., J. P. Eastwood, D. A. Brain, T. D. Phan, M. Øieroset, and R. P. Lin (2009), In situ observations of reconnection Hall magnetic fields at Mars: Evidence for ion diffusion region encounters, *J. Geophys. Res.*, *114*, A11204, doi:10.1029/2009JA014544.

Halekas, J. S., E. R. Taylor, G. Dalton, G. Johnson, D. W. Curtis, J. P. McFadden, D. L. Mitchell, R. P. Lin, and B. M. Jakosky (2013), The Solar Wind Ion Analyzer for MAVEN, *Space Sci. Rev.*, doi:10.1007/s11214-013-0029-z.

Halekas, J. S., et al. (2015), Time-dispersed ion signatures observed in the Martian magnetosphere by MAVEN, *Geophys. Res. Lett.*, *42*, doi:10.1002/2015GL064781.

Hara, T., K. Seki, H. Hasegawa, D. A. Brain, K. Matsunaga, and M. H. Saito (2014a), The spatial structure of Martian magnetic flux ropes recovered by the Grad-Shafranov reconstruction technique, *J. Geophys. Res. Space Physics*, *119*, 1262–1271, doi:10.1002/2013JA019414.

Hara, T., K. Seki, H. Hasegawa, D. A. Brain, K. Matsunaga, M. H. Saito, and D. Shiota (2014b), Formation processes of flux ropes downstream from Martian crustal magnetic fields inferred from Grad-Shafranov reconstruction, *J. Geophys. Res. Space Physics*, *119*, 7947–7962, doi:10.1002/2014JA019943.

Harada, Y., et al. (2015), Magnetic reconnection in the near-Mars magnetotail: MAVEN observations, *Geophys. Res. Lett.*, *42*, doi:10.1002/2015GL065004.

Hasegawa, H., B. U. Ö. Sonnerup, C. J. Owen, B. Klecker, G. Paschmann, A. Balogh, and H. Rème (2006), The structure of flux transfer events recovered from Cluster data, *Ann. Geophys.*, *24*, 603–618, doi:10.5194/angeo-24-603-2006.

Hasegawa, H., H. Zhang, Y. Lin, B. U. Ö. Sonnerup, S. J. Schwartz, B. Lavraud, and Q.-G. Zong (2012), Magnetic flux rope formation within a magnetosheath hot flow anomaly, *J. Geophys. Res.*, *117*, A09214, doi:10.1029/2012JA017920.

Hau, L.-N., and B. U. Ö. Sonnerup (1999), Two-dimensional coherent structures in the magnetopause: Recovery of static equilibria from single-spacecraft data, *J. Geophys. Res.*, *104*, 6899–6918, doi:10.1029/1999JA900002.

Hu, Q., and B. U. Ö. Sonnerup (2001), Reconstruction of magnetic flux ropes in the solar wind, *Geophys. Res. Lett.*, *28*, 467–470, doi:10.1029/2000GL012232.

Hu, Q., and B. U. Ö. Sonnerup (2002), Reconstruction of magnetic clouds in the solar wind: Orientations and configurations, *J. Geophys. Res.*, *107*(A7), 1142, doi:10.1029/2001JA000293.

Hu, Q., J. Qiu, B. Dasgupta, A. Khare, and G. M. Webb (2014), Structures of interplanetary magnetic flux ropes and comparison with their solar sources, *Astrophys. J.*, *793*, 53, doi:10.1088/0004-637X/793/1/53.

Jakosky, B. M., and R. J. Phillips (2001), Mars' volatile and climate history, *Nature*, *412*, 237–244, doi:10.1038/35084184.

Jakosky, B. M., et al. (2015), The Mars Atmosphere and Volatile Evolution (MAVEN) mission, *Space Sci. Rev.*, doi:10.1007/s11214-015-0139-x.

Lundin, R., H. Borg, B. Hultqvist, A. Zakharov, and R. Pellinen (1989), First measurements of the ionospheric plasma escape from Mars, *Nature*, *341*, 609–612, doi:10.1038/341609a0.

Lundin, R., S. Barabash, M. Holmström, H. Nilsson, M. Yamauchi, M. Fränz, and E. M. Dubinin (2008), A comet-like escape of ionospheric plasma from Mars, *Geophys. Res. Lett.*, *35*, L18203, doi:10.1029/2008GL034811.

Lundin, R., S. Barabash, M. Holmström, H. Nilsson, Y. Futaana, R. Ramstad, M. Yamauchi, E. Dubinin, and M. Fraenz (2013), Solar cycle effects on the ion escape from Mars, *Geophys. Res. Lett.*, *40*, 6028–6032, doi:10.1002/2013GL058154.

McFadden, J. P., et al. (2015), MAVEN Suprathermal and Thermal Ion Composition (STATIC) Instrument, *Space Sci. Rev.*

Mitchell, D. L., et al. (2015), The MAVEN Solar Wind Electron Analyzer, *Space Sci. Rev.*

Morgan, D. D., D. A. Gurnett, F. Akalin, D. A. Brain, J. S. Leisner, F. Duru, R. A. Frahm, and J. D. Winningham (2011), Dual-spacecraft observation of large-scale magnetic flux ropes in the Martian ionosphere, *J. Geophys. Res.*, *116*, A02319, doi:10.1029/2010JA016134.

Morschhauser, A., V. Lesur, and M. Grott (2014), A spherical harmonic model of the lithospheric magnetic field of Mars, *J. Geophys. Res. Planets*, *119*, 1162–1188, doi:10.1002/2013JE004555.

Nilsson, H., E. Carlsson, D. A. Brain, M. Yamauchi, M. Holmström, S. Barabash, R. Lundin, and Y. Futaana (2010), Ion escape from Mars as a function of solar wind conditions: A statistical study, *Icarus*, *206*, 40–49, doi:10.1016/j.icarus.2009.03.006.

Qiu, J., Q. Hu, T. A. Howard, and V. B. Yurchyshyn (2007), On the magnetic flux budget in low-corona magnetic reconnection and interplanetary coronal mass ejections, *Astrophys. J.*, *659*, 758–772, doi:10.1086/512060.

Russell, C. T., and R. C. Elphic (1979), Observation of magnetic flux ropes in the Venus ionosphere, *Nature*, *279*, 616–618, doi:10.1038/279616a0.

Sonnerup, B. U. Ö., and M. Guo (1996), Magnetopause transects, *Geophys. Res. Lett.*, *23*, 3679–3682, doi:10.1029/96GL03573.

Sonnerup, B. U. Ö., and M. Scheible (1998), Minimum and maximum variance analysis, in *Analysis Methods for Multi-Spacecraft Data, ISSI Sci. Rep. Ser.*, vol. 1, edited by G. Paschmann and P. Daly, pp. 185–220, Eur. Space Agency, Paris.

Sonnerup, B. U. Ö., H. Hasegawa, and G. Paschmann (2004), Anatomy of a flux transfer event seen by Cluster, *Geophys. Res. Lett.*, *31*, L11803, doi:10.1029/2004GL020134.

Sonnerup, B. U. Ö., H. Hasegawa, W.-L. Teh, and L.-N. Hau (2006), Grad-Shafranov reconstruction: An overview, *J. Geophys. Res.*, *111*, A09204, doi:10.1029/2006JA011717.

Sturrock, P. A. (1994), *Plasma Physics: An Introduction to the Theory of Astrophysical, Geophysical and Laboratory Plasmas, Stanford-Cambridge Program*, Cambridge Univ. Press, Cambridge, U. K.

Vignes, D., M. H. Acuña, J. E. P. Connerney, D. H. Crider, H. Rème, and C. Mazelle (2004), Magnetic flux ropes in the Martian atmosphere: Global characteristics, *Space Sci. Rev.*, *111*, 223–231, doi:10.1023/B:SPAC.0000032716.21619.f2.